Title

IFITM proteins assist cellular uptake of diverse linked chemotypes

Journal

Science, 378(6624)

ISSN

0036-8075

Authors

Lou, Kevin
Wassarman, Douglas R
Yang, Tangpo
et al.

Publication Date

2022-12-09

DOI

10.1126/science.abl5829

HHS Public Access

Author manuscript

Science. Author manuscript; available in PMC 2023 February 13.

Published in final edited form as:

Science. 2022 December 09; 378(6624): 1097–1104. doi:10.1126/science.abl5829.

IFITM proteins assist cellular uptake of diverse linked chemotypes

Kevin Lou[1,2], **Douglas R. Wassarman**[1,2], **Tangpo Yang**[1], **YiTing Paung**[3], **Ziyang Zhang**[1,2,4], **Thomas A. O'Loughlin**[5,6], **Megan K. Moore**[1,2], **Regina K. Egan**[7], **Patricia Greninger**[7], **Cyril H. Benes**[7,8], **Markus A. Seeliger**[3], **Jack Taunton**[1], **Luke A. Gilbert**[5,6,9,10,*], **Kevan M. Shokat**[1,2,4,*]

[1]Department of Cellular and Molecular Pharmacology, University of California, San Francisco, San Francisco, CA 94158, United States.

[2]Howard Hughes Medical Institute, University of California, San Francisco, San Francisco, CA 94158, United States.

[3]Department of Pharmacological Sciences, Stony Brook University, Stony Brook, New York 11794-8651, United States.

[4]Department of Chemistry, University of California, Berkeley, Berkeley, 94720, CA, United States.

[5]Helen Diller Family Comprehensive Cancer Center, University of California, San Francisco, San Francisco, CA 94158, United States.

[6]Department of Urology, University of California, San Francisco, San Francisco, CA 94158, United States.

[7]Center for Cancer Research, Massachusetts General Hospital Cancer Center, Charlestown, MA 02129, United States.

[8]Department of Medicine, Harvard Medical School, Boston, MA 02115, United States.

[9]Innovative Genomics Institute, University of California, San Francisco, San Francisco, CA 94158, United States.

[10]Arc Institute, Palo Alto, CA, 94304, United States.

*Corresponding author. kevan.shokat@ucsf.edu (K.M.S.); luke@arcinstitute.org (L.A.G.).

Author contributions: K.L., L.A.G., and K.M.S. were responsible for the conception, design, and interpretation of the experiments and wrote the manuscript. K.L. performed CRISPRi/a experiments, cellular uptake assays, and chemical-genetic interaction mapping. K.L. designed and synthesized DasatiLink and BisRoc molecules. D.R.W., R.K.E., and P.G. performed sensitivity-expression correlation experiments. T.Y. performed chemoproteomic kinase target engagement assays. Y.P. performed protein NMR spectroscopy. Z.Z. designed and synthesized TAMRA molecules. T.A.O. performed fluorescent microscopy experiments. M.K.M. performed biological validation of BisRoc experiments. C.H.B., M.A.S., J.T., L.A.G., and K.M.S. supervised experiments and interpreted data. All authors edited the manuscript.

Competing interests: K.L. and K.M.S. have filed a patent application covering DasatiLink analogs. K.L., M.K.M., and K.M.S. have filed a patent application covering BisRoc analogs. Kin of K.L. hold stock in and are employed by Pharmaron. C.H.B. is currently an employee of Novartis. J.T. is a founder of Global Blood Therapeutics, Principia Biopharma, Kezar Life Sciences, Cedilla Therapeutics, and Terremoto Biosciences, and is a scientific advisor to Entos. L.A.G. has filed patent applications related to CRISPRi/a screening. K.M.S. has filed patent applications covering RapaLink analogs which are licensed to Revolution Medicines. K.M.S. receives stock and cash compensation from Revolution Medicines.

Abstract

The search for cell permeable drugs has conventionally focused on low molecular weight, non-polar, and rigid chemical structures. However, emerging therapeutic strategies break traditional drug design rules by employing flexibly linked chemical entities composed of more than one ligand. Using complementary genome-scale chemical-genetic approaches we identified an endogenous chemical uptake pathway involving interferon induced transmembrane proteins (IFITMs) that modulates the cell permeability of a prototypical biopic inhibitor of MTOR (RapaLink-1, MW: 1784 g/mol). We devised additional linked inhibitors targeting BCR-ABL1 (DasatiLink-1, MW: 1518 g/mol) and EIF4A1 (BisRoc-1, MW: 1466 g/mol) whose uptake was facilitated by IFITMs. We also found that IFITMs moderately assisted some proteolysis targeting chimeras (PROTACs) and examined the physicochemical requirements for involvement of this uptake pathway.

1 sentence summary:

Chemical-genetic approaches elucidate uptake pathway for molecules breaking traditional drug design rules.

Any therapeutic molecule that binds to an intracellular target must first cross the cell membrane. Retrospective analyses of compound libraries and their biological activities have yielded empirical guidelines (e.g. Lipinski's rule of five) that enrich for lead-like scaffolds with high passive permeability and largely define modern drug-like chemical space (1–3). While these principles have been useful for streamlining the search for new therapeutics, many important intracellular drug targets are currently refractory to inhibition by these compact, hydrophobic, and rigid molecules. An emerging design framework that seeks to address these challenges involves increasing pharmacological complexity by linking multiple ligands into a single chemical entity (a linked chemotype). Linked chemotypes can have enhanced potency, greater selectivity, and the capacity to induce the association of more than one target (4–11). This modular rapid access to high molecular weight, amphiphilicity, and rotational flexibility can provide useful chemical probes and therapeutic leads for intracellular targets, as long as the resulting molecules remain cell permeable.

Mechanisms to understand and predict the cell permeability of linked chemotypes, however, remain limited. Other medium-to-high molecular weight therapeutics such as natural products and synthetic macrocycles often comprise highly tailored arrangements of polar/non-polar functionality that allow switching between membrane-favored and aqueous-favored conformations to enable passive permeability through membranes (12). Additionally, cell penetrating proteins/peptides commonly require appendage of highly charged moieties to enable electrostatic interactions with the plasma membrane and subsequent internalization (13–15). Studies involving the most rapidly expanding linked chemotype class, proteolysis targeting chimeras (PROTACs) (16), provide varying insights into the determinants of cell permeability (17–22). Despite their atypical properties, PROTACs and additional large molecules such as the dimeric immunophilin ligand rimiducid have shown in-cell activity robust enough to enter clinical trials (16, 23).

Given this discrepancy between the favorable biological activity of many large, bivalent molecules and traditional concepts of passive permeability, we inferred that linked chemotypes might hijack cellular processes to assist with passage through the cell membrane. We selected as an example a bitopic inhibitor of MTOR, RapaLink-1 (7), whose molecular weight (1784 g/mol) falls well beyond common guidelines (≤ 500 g/mol) (1), and even beyond that of typical PROTACs (800–1200 g/mol) (table S1) (18). RapaLink-1's atypical structure, composed of the allosteric MTOR inhibitor rapamycin and the active-site inhibitor sapanisertib linked by an 8-unit polyethylene glycol (PEG8) tether (Fig. 1A), confers enhanced selectivity for MTOR complex 1 over MTOR complex 2 (7, 24, 25). The molecule is highly active *in vivo*, penetrates the blood-brain barrier, and serves as a prototype for the clinical candidate RMC-5552 (7, 24–27), establishing itself as a drug-like compound that defies most traditional notions of drug-like structure. We hypothesized that cellular mechanisms assisting RapaLink-1's cytoplasmic entry could be identified by systematically perturbing genes that modulate the molecule's ability to reach and inhibit its intracellular target.

Complementary genome-scale chemical-genetic approaches identify IFITMs as regulators of RapaLink-1 cellular activity

We probed canonical protein coding genes for cellular factors that determine RapaLink-1 uptake and sensitivity using a dCas9-based CRISPRi/a functional genomics platform (28, 29). Gene expression inhibition and activation, through CRISPRi and CRISPRa respectively, act as complementary approaches to map chemical-genetic interactions at genome-scale. In particular, genes displaying strong mirrored phenotypes (resistance upon knockdown and sensitivity upon overexpression) are likely to be directly involved in a small molecule's mechanism of action. This integrated approach to identifying physiologically relevant chemical-genetic interactions was proposed by Jost et al. and its utility has recently been reviewed (30, 31). In addition to the bitopic inhibitor, we also assessed sapanisertib, rapamycin, and an unlinked control (a 1:1 mixture of sapanisertib and rapamycin) to distinguish chemical-genetic interactions specific to the linked chemotype (Fig. 1A).

Patient-derived chronic myeloid leukemia (CML) cells, K562, pre-engineered to express CRISPRi or CRISPRa machinery, were transduced with their respective genome-scale sgRNA libraries, selected with puromycin to remove non-transduced cells, and treated with DMSO, sapanisertib, rapamycin, sapanisertib + rapamycin, or RapaLink-1. The experiments were conducted with high replicate reproducibility (fig. S1, A to D), and data from the genome-scale CRISPRi (data file S1 and data file S2) and CRISPRa (data file S3 and data file S4) screens were juxtaposed to highlight genes that displayed mirrored phenotypes (Fig. 1B). This arrangement distributes genes which functionally synergize with the inhibitor in the lower right (e.g. *FKBP12*, the required inhibitory complex partner of rapamycin) and those which antagonize the inhibitor in the upper left (e.g. *MTOR*, the direct target) (30, 31). Chemical-genetic interactions with MTOR signaling components, particularly the Ragulator complex (*RRAGA*, *RRAGC*, and *LAMTOR1–5*) and nodes downstream of PI3K/AKT (*TSC1*, *TSC2*, and *RHEB*), were observed across multiple inhibitor conditions (fig. S2, A

and B), consistent with known pathway relationships (32) and prior functional genomics studies (33, 34).

A distinct set of chemical-genetic interactions were identified as top hits with RapaLink-1 and not with any of the non-linked molecules tested, suggesting the involvement of a biological pathway that promotes the activity of the linked chemotype. The expression of members of a highly homologous gene family, interferon induced transmembrane proteins (IFITMs) *IFITM1*, *IFITM2*, and *IFITM3* (35), synergized with the activity of RapaLink-1 and not its non-linked counterparts, sapanisertib and rapamycin (Fig. 1B). To validate this finding, we tested sgRNAs targeting *IFITM1–3* individually for transcriptional repression or activation (fig. S3A and table S2). CRISPRi-mediated knockdown of *IFITM1–3* was potent and selective (fig. S3B). CRISPRa-mediated overexpression was also potent although we observed variable cross activation between family members (fig. S3C), possibly due to concerted transcriptional regulation of these genes, which are adjacent to each other on chromosome 11 (fig. S3A) (36). We individually confirmed that top screen hits, including *FKBP12* and *IFITM1–3*, synergized with RapaLink-1 in a competitive growth assay and also validated that the *IFITM1–3* chemical-genetic interaction was specific to the linked chemotype (fig. S3, D and E).

Seeking to generalize these observations beyond a single cell type, we employed an independent chemical-genetic approach correlating MTOR inhibitor sensitivity data with basal gene expression in diverse *in vitro* models (37–39). Over 500 cancer cell lines were assessed for sensitivity to sapanisertib, rapamycin, or RapaLink-1 (measured by area under the dose-response curve). These measurements were correlated with gene transcript abundance (measured by RNA sequencing) across the cell lines to identify predictive biomarkers for compound sensitivity or resistance. High expression of any of the three IFITM family members was strongly associated with enhanced RapaLink-1 sensitivity across 659 cell lines, and *IFITM2* was notably the single most associated sensitizing biomarker (negative correlation) for Rapalink-1 (Fig. 1C and data file S5). This correlation was absent for sapanisertib and rapamycin (fig. S4, A to C, and data file S5), recapitulating the CRISPRi/a screens. Together, our analysis of the CRISPRi/a screens and large-scale chemogenomic cell line profiling experiments suggested a role of IFITMs in promoting the activity of RapaLink-1 across diverse cell types and levels of IFITM expression.

IFITMs promote RapaLink-1 pharmacodynamic target engagement

To unmask potentially overlapping IFITM functions, we knocked down *IFITM1*, *IFITM2*, and *IFITM3* expression simultaneously by co-expressing three different targeting sgRNAs (table S2) (40). While multigene knockdown was potent (fig. S5A), we did not observe baseline changes in cell viability (fig. S5B). *IFITM1–3* triple knockdown ablated MTOR inhibition by 3 nM RapaLink-1 in cells, as determined by intracellular markers of MTOR pathway signaling, phospho-S6$^{S235/236}$, phospho-4EBP1$^{T37/46}$, and phospho-AKT^{S473} (Fig. 1D), and conferred resistance to the linked molecule (Fig. 1E and fig. S5C). Overall, IFITM expression perturbation by CRISPRi and CRISPRa caused a combined 29.5-fold modulation in cellular potency of the molecule (Fig. 1, E and F). As has been observed previously (7), RapaLink-1 requires multiple hours to achieve maximal pharmacodynamic inhibition (Fig.

1D). This contrasts with the typical finding that small molecules reach their intracellular targets on the seconds-to-minutes timescale (41) and may reflect how linked chemotypes exhibit distinct permeability characteristics from traditional drug-like molecules.

Neither of the non-linked MTOR inhibitors tested demonstrated chemical-genetic interactions with *IFITM1–3*, thus IFITMs likely do not directly modulate MTOR signaling, but instead cooperate with some aspect of RapaLink-1 not shared with the other inhibitors. Clade I IFITM family members, *IFITM1–3*, are closely related broad spectrum viral restriction factors that localize to the plasma and endolysosomal membranes (42–45). They are thought to perform their antiviral function, in part, by rendering local membrane characteristics at the viral-endosomal juncture unfavorable for viral entry (46), although in some cases viruses can also hijack IFITMs to facilitate entry and infection (47). In addition to their established immunologic function, clade I IFITMs are also reported to modulate an oncogenic phenotype (48), affect placenta formation (49), and contribute to cellular homeostasis (44). In turn, Rapalink-1 might interact with IFITMs through a cellular pathway that promotes the uptake of the large molecule.

A fluorescent RapaLink-1 analog reveals a role for IFITMs in linked chemotype uptake

To explore our uptake hypothesis, we created a fluorescent analog of RapaLink-1 to directly observe the effect of IFITM expression on accumulation of the linked chemotype in live cells. This fluorescent molecule, RapaTAMRA-PEG8, was designed by replacing the adenosine triphosphate (ATP)-site binding element in RapaLink-1 with tetramethylrhodamine (TAMRA), resulting in a fluorescent derivative that closely mimics the physicochemical properties of the original molecule (Fig. 2A and table S1) (27). Analogs representing partial components of RapaTAMRA-PEG8, TAMRA-N_3 and TAMRA-PEG8-N_3, were additionally evaluated to assess whether the uptake pathway extended to generic compact-hydrophobic or linked-amphiphilic chemotypes respectively (Fig. 2A). We quantified accumulation of these molecules by flow cytometry using a quantitative live cell fluorescence uptake assay in which a mixture of transduced (sgRNA+) and non-transduced (sgRNA-) cells were equally exposed to compound within the same well (Fig. 2B and fig. S6A). Changes in cellular uptake resulting from CRISPRi/a expression modulation by sgRNAs (fig. S3, A to C) again revealed a chemotype-specific IFITM dependency pattern (Fig. 2, B and C, and fig. S6A). Both linked chemotypes, TAMRA-PEG8-N_3 and RapaTAMRA-PEG8, demonstrated decreased uptake upon knockdown of *IFITM1–3* and increased uptake upon overexpression. The linker-less chemotype, TAMRA-N_3, in contrast exhibited no such chemical-genetic interactions. CRISPRi/a-induced uptake differences observed for RapaTAMRA-PEG8 correlated strongly with resistance and sensitivity phenotypes for RapaLink-1 (fig. S6B), suggesting a direct association between measured uptake and functional target inhibition. The observation that uptake of TAMRA-PEG8-N_3, a generic linked chemotype not specifically bound by any cellular protein, was also IFITM-assisted suggested that this uptake mechanism might also be used by other linked molecules.

Additionally, we assessed the role of IFITMs on the subcellular localization of RapaTAMRA-PEG8 by confocal microscopy in a human non-transformed cell line, RPE-1, pre-engineered to express CRISPRi machinery. Again a mixture of sgRNA+ and sgRNA- cells were imaged in the same well following equal exposure to fluorescent compound. *IFITM1–3* triple-knockdown significantly reduced the amount of RapaTAMRA-PEG8 entering the intracellular compartment (Fig. 2D and fig. S6C). A reduction in signal was also observed within the endolysosomal compartment (Fig. 2D and fig. S6C), suggesting that IFITMs, which localize to the plasma membrane as well as endolysosomal membranes (43–45), may play a role in facilitating RapaTAMRA-PEG8 uptake through endocytic vesicles and into the intracellular space. Consistent with this, our functional genomics screens identified RapaLink-1-specific chemical-genetic interactions among endosomal (*ARF6*, *VPS26A*, *VPS29*, and *VPS35*) and sterol (*OSBP*, *GRAMD1A*, *INSIG1*, and *SCAP*) regulatory genes (fig. S7, A and B). This, in part, resembles IFITMs' roles as antiviral effectors in which biophysical interactions with incoming viral particles (50) and membrane sterols (51) may hinder or assist infection of target cells (43–45). Considering the large diversity of viruses IFITMs are described to interact with, we hypothesized that the uptake assistance afforded to RapaLink-1 and RapaTAMRA-PEG8 by IFITMs might also extend to other linked chemotypes with similar physicochemical properties.

DasatiLink-1 is an IFITM-assisted bitopic inhibitor of BCR-ABL1 with enhanced selectivity

To explore the generalizability of this IFITM-promoted cellular uptake mechanism, we designed, synthesized, and characterized a bitopic inhibitor that is, aside from being a linked molecule, compositionally unrelated to RapaLink-1. This inhibitor targets a different intracellular protein, BCR-ABL1, a fusion oncoprotein associated with CML and other leukemias (52). BCR-ABL1 harbors two well-defined small molecule binding sites within its kinase domain (Fig. 3A): the ATP pocket (53), which is targeted by five clinically approved compounds (e.g. dasatinib) (54), and the myristoyl pocket (55), which is targeted by the clinical inhibitor asciminib (56). These sites can also be bound by the two classes of inhibitors simultaneously (55–57). The two pockets span a similar distance as those engaged by RapaLink-1 in MTOR (7), suggesting that a similar bitopic inhibitor linkage strategy could apply to BCR-ABL1. We devised a bitopic inhibitor of BCR-ABL1, DasatiLink-1, based on the linking of dasatinib and asciminib by a flexible tether whose length (41 heavy atoms) was close to that of RapaLink-1 (39 heavy atoms) (Fig. 3B).

We characterized the interaction between DasatiLink-1 and its target using *in vitro* biochemical assays. Treatment of purified BCR-ABL1 kinase domain with dasatinib or asciminib caused marked (> 0.1 ppm) nuclear magnetic resonance (NMR) chemical shift differences in residues involved in binding to the monomeric inhibitors (fig. S8, A and B), consistent with previous reports (55, 56, 58). The NMR spectrum observed in the presence of Dasatilink-1 closely matched the spectrum observed with a mixture of the two non-linked inhibitors (fig. S8, A and B), suggesting that the linked inhibitor simultaneously binds to both sites and that the tether does not prevent binding to either site.

We hypothesized that DasatiLink-1 might require an allosteric foothold to achieve high occupancy of the BCR-ABL1 kinase domain, and we tested this hypothesis using a pulldown assay for ATP-site availability (59). We confirmed that the assay recapitulated a biochemical IC_{50} of < 1 nM for dasatinib (60), which was unaffected by inclusion of 100-fold excess of the allosteric inhibitor asciminib (fig. S8C). However, addition of excess asciminib impaired the ability of DasatiLink-1 to occupy the ATP-site, likely resulting from a loss of avidity following steric occlusion of the allosteric pocket (fig. S8C). This indicates that Dasatilink-1 relies on both the orthosteric and allosteric sites for binding, suggesting that it might also exhibit the enhanced selectivity often observed in bitopic inhibitors (61). Together, these biochemical data validate DasatiLink-1 as a bitopic inhibitor with physicochemical properties beyond standard drug design limits (1–3), and we reasoned that the molecule's linked composition might allow it to be assisted into the cell by IFITMs.

Returning to our K562 CRISPRi/a models, which are patient-derived BCR-ABL1 mutant CML cells, we characterized the effect of IFITM expression on the ability of DasatiLink-1 to inhibit intracellular BCR-ABL1 signaling. Similar to RapaLink-1 (Fig. 1, E and F), CRISPRi and CRISPRa perturbation of IFITM expression resulted in a combined 8.9-fold modulation of DasatiLink-1 cellular potency (Fig. 3, C and D). We also probed the capacity of DasatiLink-1 to engage intracellular BCR-ABL1 by measuring pharmacodynamic markers of inhibition. Consistent with an IFITM-assisted uptake mechanism, *IFITM1–3* triple knockdown reduced the ability of DasatiLink-1 to inhibit phospho-BCR-ABL1^{Y245} and phospho-STAT5^{Y694}, which are known BCR-ABL1 substrates (Fig. 3E). The maximal inhibition observed for DasatiLink-1 in the TriNegCtrl sg conditions at 8 and 24 h was not ever reached in the *IFITM1–3* triple knockdown conditions, likely due to lower intracellular concentrations of compound resulting from decreased uptake. The inhibition kinetics we observed for the negative control treatment, requiring multiple hours for maximal inhibition at a nanomolar concentration (Fig. 3E), were also exhibited by RapaLink-1 (Fig. 1D).

We anticipated that DasatiLink-1, akin to RapaLink-1, was likely to be selective for its target as a result of its multivalent binding mechanism – only BCR-ABL1 kinase domain contains binding sites for both of its linked components. We assessed DasatiLink-1's kinome-wide selectivity in live cells using a promiscuous kinase occupancy probe, XO44 (62), with which kinase active-site occupancy can be determined through competitive activity-based protein profiling (63). In contrast to an unlinked control (a 1:1 mixture of dasatinib and asciminib) at equimolar concentration, which competed with XO44 for labeling of numerous known dasatinib targets (62), pretreatment with DasatiLink-1 resulted in observable intracellular occupancy of only ABL1 (Fig. 3F, data file S6). This single kinase specificity extended over a 100-fold concentration range up to 1 μM, the same range over which the unlinked control demonstrated dose-responsive occupancy of numerous off-targets (Fig. 3G, data file S6). These data suggest that target selectivity can be conferred by two-site binding, analogous to RapaLink-1's selectivity for MTOR complex 1 (7, 24, 25).

BisRoc-1 analogs reveal linker length dependency of IFITM-assisted cellular uptake

To further examine the breadth of linked chemotypes that might be assisted by IFITMs, we designed, synthesized, and characterized a new linked molecular glue inhibitor based on the natural product rocaglamide. Rocaglamide clamps the EIF4A1 helicase to 5' untranslated regions (UTRs) of target mRNAs to inhibit the translation of downstream sequences (64). The crystal structure of the complex of rocaglamide, EIF4A1, and polypurine RNA (65) revealed that the molecule's amide points toward free solvent, near a symmetry mate (fig. S9A). We reasoned that dimerization of rocaglamide through its amide position could be a chemically tractable means to simultaneously engage two proximal EIF4A1-RNA complexes within the cell. We designed a molecule, BisRoc-1 (fig. S9B), that links two rocaglamide monomers together with a linker length (35 heavy atoms) exceeding the distance separating two rocaglamide binding sites in the crystal structure (fig. S9A). Similar to RapaLink-1 and DasatiLink-1, CRISPRi and CRISPRa perturbation of IFITM expression resulted in a combined 6.2-fold modulation in cellular activity of BisRoc-1 (fig. S9, C and D). Additionally, we evaluated the relationship between linker length and IFITM assistance by examining an analog series consisting of BisRoc-1 (PEG11), BisRoc-2 (PEG4), BisRoc-3 (PEG2), and rocaglamide (no linker) (fig. S9E). We treated our K562 CRISPRi and CRISPRa cells with these inhibitors and evaluated differences in potency resulting from IFITM expression modulation, as measured by half-maximal inhibitory concentration (IC_{50}) shift in a cell viability assay (fig. S9, E and F, and data file S7). This revealed a pattern in which longer linker lengths correlated with greater IFITM assistance. Combined, these data suggest the general feasibility of retaining cell permeability despite increased pharmacophore size, polarity, and flexibility in the context of linked chemotypes described herein.

An expanded chemical space for cell permeable molecules

Given the ubiquitous presence of IFITMs in cells, we hypothesized that the cellular uptake of other linked inhibitors in the literature could also be assisted by IFITMs. While not generally as large as the linked chemotypes described above, PROTACs are likewise composed of two chemical entities covalently attached by a flexible tether (16). Thus, we included four PROTACs (GMB-475, MZ1, BETd-260, and dBET6) and their non-linked parent inhibitors in an expanded survey of chemical-genetic interactions with IFITMs (Fig. 4A, fig. S10, and table S1). These compounds were evaluated in the same IFITM dependency analysis as the BisRoc linker series (Fig. 4B and data file S7). Using RapaLink-1 as a chemical benchmark, we observed that *IFITM1*, *IFITM2*, and *IFITM3* overexpression sensitized cells to linked chemotypes (Fig. 4B; compounds 9-17). The inverse finding, resistance to linked chemotypes, resulted from gene knockdown (Fig. 4B). The trend observed in the BisRoc series was corroborated across the 9 bivalent molecules tested (Fig. 4B): the magnitudes of chemical-genetic interactions correlated with linker length which is reflected in inhibitor size (molecular weight) and flexibility (number of rotatable bonds). Linked chemotypes with long linkers were more IFITM-assisted than linked chemotypes with short linkers, and non-linked chemotypes (Fig. 4B; compounds

1-8) were not observed to be assisted by IFITMs (Fig. 4B). Despite their cellular activities, the physicochemical properties of the linked chemotypes largely violate Lipinski's (1) and Veber's (2) classic guidelines (Fig. 4, A to C, and table S1), raising the need for a revised drug design framework that considers IFITM-assisted uptake and other cellular import processes.

Discussion

Through a combination of functional genomics and chemical methods, we uncovered an endogenous pathway involving IFITMs that in our data promotes the cellular uptake of diverse linked chemotypes. With the clinical advancement of a dimeric immunophilin ligand (23), PROTACs (16), and a RapaLink-1 derivative (26), the notion of 'drug-like' is continually being revised. As evidence, the chemical space (66) populated by an ever-expanding set of linked preclinical compounds in the literature ventures beyond that occupied by lead inhibitors developed under traditional guidelines (Fig. 4C) (1–3). Here, we identify IFITM-assisted cellular uptake as one of the mechanisms by which linked inhibitors are able to break previously established rules surrounding drug-likeness. We anticipate that our findings will inform the uptake optimization of emerging classes of bivalent molecules (PROTACs, Syn-TEFs, RIBOTACs, PHICS, DUBTACs, and others) (4–11) and enable the design of cell permeable therapeutics that bridge distal binding sites on solitary targets or multi-target complexes.

Supplementary Material

Refer to Web version on PubMed Central for supplementary material.

Acknowledgements

Sequencing was performed at the UCSF CAT, supported by UCSF PBBR, RRP IMIA, and NIH 1S10OD028511–01 grants. We thank Taia S. Wu for computational advice, SoYeon Kim and Kari Herrington at the UCSF Nikon Imaging Center for their microscopy assistance and expertise, D. Matthew Peacock for assistance acquiring NMR characterization of compounds synthesized herein, and Jack W. Stevenson for proofreading.

Funding:

This work was supported by NIH grant F30CA239476 (to K.L.); NIH grant F31CA243439 (to D.R.W.); Damon Runyon Cancer Research Foundation fellowship DRG-2281–17 (to Z.Z.); Wellcome Trust grant 102696 (to C.H.B.); NIH grant R35GM119437 (to M.A.S.); Ono Pharma Foundation and Pfizer (to J.T.); NIH New Innovator Award DP2-CA239597, a Pew-Stewart Scholars for Cancer Research award, and the Goldberg-Benioff Endowed Professorship in Prostate Cancer Translational Biology (to L.A.G.); the Howard Hughes Medical Institute, the Samuel Waxman Cancer Research Foundation, and NIH grants 1R01CA221969 and 1U19 AI171110–01 (to K.M.S.).

Data and materials availability:

All data are available in the manuscript or the supplementary materials. Scripts implementing analyses are available at https://github.com/dwassarman, https://github.com/mhorlbeck, and Zenodo (67, 68). Materials are available upon request to the corresponding authors with a signed material transfer agreement.

References

1. Lipinski CA, Lombardo F, Dominy BW, Feeney PJ, Experimental and computational approaches to estimate solubility and permeability in drug discovery and development settings. Adv Drug Deliver Rev. 23, 3–25 (1997).
2. Veber DF, Johnson SR, Cheng H-Y, Smith BR, Ward KW, Kopple KD, Molecular Properties That Influence the Oral Bioavailability of Drug Candidates. J Med Chem. 45, 2615–2623 (2002). [PubMed: 12036371]
3. Ghose AK, Viswanadhan VN, Wendoloski JJ, A Knowledge-Based Approach in Designing Combinatorial or Medicinal Chemistry Libraries for Drug Discovery. 1. A Qualitative and Quantitative Characterization of Known Drug Databases. J Comb Chem. 1, 55–68 (1999). [PubMed: 10746014]
4. Erez M, Takemori AE, Portoghese PS, Narcotic antagonistic potency of bivalent ligands which contain .beta.-naltrexamine. Evidence for simultaneous occupation of proximal recognition sites. J Med Chem. 25, 847–849 (1982). [PubMed: 7108900]
5. Spencer D, Wandless T, Schreiber S, Crabtree G, Controlling signal transduction with synthetic ligands. Science. 262, 1019–1024 (1993). [PubMed: 7694365]
6. Sakamoto KM, Kim KB, Kumagai A, Mercurio F, Crews CM, Deshaies RJ, Protacs: Chimeric molecules that target proteins to the Skp1-Cullin-F box complex for ubiquitination and degradation. Proc National Acad Sci. 98, 8554–8559 (2001).
7. Rodrik-Outmezguine VS, Okaniwa M, Yao Z, Novotny CJ, McWhirter C, Banaji A, Won H, Wong W, Berger M, de Stanchina E, Barratt DG, Cosulich S, Klinowska T, Rosen N, Shokat KM, Overcoming mTOR resistance mutations with a new-generation mTOR inhibitor. Nature. 534, 272–6 (2016). [PubMed: 27279227]
8. Erwin GS, Grieshop MP, Ali A, Qi J, Lawlor M, Kumar D, Ahmad I, McNally A, Teider N, Worringer K, Sivasankaran R, Syed DN, Eguchi A, Ashraf Md., Jeffery J, Xu M, Park PMC, Mukhtar H, Srivastava AK, Faruq M, Bradner JE, Ansari AZ, Synthetic transcription elongation factors license transcription across repressive chromatin. Science. 358, eaan6414 (2017).
9. Costales MG, Matsumoto Y, Velagapudi SP, Disney MD, Small Molecule Targeted Recruitment of a Nuclease to RNA. J Am Chem Soc. 140, 6741–6744 (2018). [PubMed: 29792692]
10. Siriwardena SU, Godage DNPM, Shoba VM, Lai S, Shi M, Wu P, Chaudhary SK, Schreiber SL, Choudhary A, Phosphorylation-Inducing Chimeric Small Molecules. J Am Chem Soc. 142, 14052–14057 (2020). [PubMed: 32787262]
11. Henning NJ, Boike L, Spradlin JN, Ward CC, Liu G, Zhang E, Belcher BP, Brittain SM, Hesse MJ, Dovala D, McGregor LM, Misiolek RV, Plasschaert LW, Rowlands DJ, Wang F, Frank AO, Fuller D, Estes AR, Randal KL, Panidapu A, McKenna JM, Tallarico JA, Schirle M, Nomura DK, Deubiquitinase-targeting chimeras for targeted protein stabilization. Nat Chem Biol. 18, 412–421 (2022). [PubMed: 35210618]
12. Doak BC, Over B, Giordanetto F, Kihlberg J, Oral Druggable Space beyond the Rule of 5: Insights from Drugs and Clinical Candidates. Chem Biol. 21, 1115–1142 (2014). [PubMed: 25237858]
13. Green M, Loewenstein PM, Autonomous functional domains of chemically synthesized human immunodeficiency virus tat trans-activator protein. Cell. 55, 1179–1188 (1988). [PubMed: 2849509]
14. Frankel AD, Pabo CO, Cellular uptake of the tat protein from human immunodeficiency virus. Cell. 55, 1189–1193 (1988). [PubMed: 2849510]
15. Snyder EL, Dowdy SF, Cell Penetrating Peptides in Drug Delivery. Pharmaceut Res. 21, 389–393 (2004).
16. Békés M, Langley DR, Crews CM, PROTAC targeted protein degraders: the past is prologue. Nat Rev Drug Discov. 21, 181–200 (2022). [PubMed: 35042991]
17. Foley CA, Potjewyd F, Lamb KN, James LI, Frye SV, Assessing the Cell Permeability of Bivalent Chemical Degraders Using the Chloroalkane Penetration Assay. Acs Chem Biol. 15, 290–295 (2019). [PubMed: 31846298]

18. Cantrill C, Chaturvedi P, Rynn C, Schaffland JP, Walter I, Wittwer MB, Fundamental aspects of DMPK optimization of targeted protein degraders. Drug Discov Today. 25, 969–982 (2020). [PubMed: 32298797]
19. Scott DE, Rooney TPC, Bayle ED, Mirza T, Willems HMG, Clarke JH, Andrews SP, Skidmore J, Systematic Investigation of the Permeability of Androgen Receptor PROTACs. Acs Med Chem Lett (2020), doi:10.1021/acsmedchemlett.0c00194.
20. Ermondi G, Vallaro M, Caron G, Degraders early developability assessment: face-to-face with molecular properties. Drug Discov Today. 25, 1585–1591 (2020). [PubMed: 32565163]
21. Klein VG, Townsend CE, Testa A, Zengerle M, Maniaci C, Hughes SJ, Chan K-H, Ciulli A, Lokey RS, Understanding and Improving the Membrane Permeability of VH032-Based PROTACs. Acs Med Chem Lett. 11, 1732–1738 (2020). [PubMed: 32939229]
22. Atilaw Y, Poongavanam V, Nilsson CS, Nguyen D, Giese A, Meibom D, Erdelyi M, Kihlberg J, Solution Conformations Shed Light on PROTAC Cell Permeability. Acs Med Chem Lett. 12, 107–114 (2020). [PubMed: 33488971]
23. Stasi AD, Tey S-K, Dotti G, Fujita Y, Kennedy-Nasser A, Martinez C, Straathof K, Liu E, Durett AG, Grilley B, Liu H, Cruz CR, Savoldo B, Gee AP, Schindler J, Krance RA, Heslop HE, Spencer DM, Rooney CM, Brenner MK, Inducible Apoptosis as a Safety Switch for Adoptive Cell Therapy. New Engl J Medicine. 365, 1673–1683 (2011).
24. Fan Q, Aksoy O, Wong RA, Ilkhanizadeh S, Novotny CJ, Gustafson WC, Truong AY-Q, Cayanan G, Simonds EF, Haas-Kogan D, Phillips JJ, Nicolaides T, Okaniwa M, Shokat KM, Weiss WA, A Kinase Inhibitor Targeted to mTORC1 Drives Regression in Glioblastoma. Cancer Cell. 31, 424–435 (2017). [PubMed: 28292440]
25. Lee BJ, Boyer JA, Burnett GL, Thottumkara AP, Tibrewal N, Wilson SL, Hsieh T, Marquez A, Lorenzana EG, Evans JW, Hulea L, Kiss G, Liu H, Lee D, Larsson O, McLaughlan S, Topisirovic I, Wang Z, Wang Z, Zhao Y, Wildes D, Aggen JB, Singh M, Gill AL, Smith JAM, Rosen N, Selective inhibitors of mTORC1 activate 4EBP1 and suppress tumor growth. Nat Chem Biol. 17, 1065–1074 (2021). [PubMed: 34168367]
26. III HAB, Ulahannan SV, Haura EB, Ou S-HI, Capasso A, Munster PN, Kitai H, Wang Z, Hayes J, Tao L, Wong S, Yang YC, Jiang J, Bitman B, Singh M, Gustafson WC, Rosen N, Schram AM, The bi-steric mTORC1-selective inhibitor RMC-5552 in tumors with activation of mTOR signaling: Preclinical activity in combination with RAS(ON) inhibitors in RAS-addicted tumors, and initial clinical findings from a single agent phase 1/1b study. J Clin Oncol. 40, 3098–3098 (2022). [PubMed: 36070625]
27. Zhang Z, Fan Q, Luo X, Lou K, Weiss WA, Shokat KM, Brain-restricted mTOR inhibition with binary pharmacology. Nature, in press.
28. Gilbert LA, Horlbeck MA, Adamson B, Villalta JE, Chen Y, Whitehead EH, Guimaraes C, Panning B, Ploegh HL, Bassik MC, Qi LS, Kampmann M, Weissman JS, Genome-Scale CRISPR-Mediated Control of Gene Repression and Activation. Cell. 159, 647–661 (2014). [PubMed: 25307932]
29. Horlbeck MA, Gilbert LA, Villalta JE, Adamson B, Pak RA, Chen Y, Fields AP, Park C, Corn JE, Kampmann M, Weissman JS, Compact and highly active next-generation libraries for CRISPR-mediated gene repression and activation. eLife. 5, e19760 (2016).
30. Jost M, Chen Y, Gilbert LA, Horlbeck MA, Krenning L, Menchon G, Rai A, Cho MY, Stern JJ, Prota AE, Kampmann M, Akhmanova A, Steinmetz MO, Tanenbaum ME, Weissman JS, Combined CRISPRi/a-Based Chemical Genetic Screens Reveal that Rigosertib Is a Microtubule-Destabilizing Agent. Molecular Cell. 68, 210–223.e6 (2017). [PubMed: 28985505]
31. Jost M, Weissman JS, CRISPR Approaches to Small Molecule Target Identification. Acs Chem Biol. 13, 366–375 (2018). [PubMed: 29261286]
32. Liu GY, Sabatini DM, mTOR at the nexus of nutrition, growth, ageing and disease. Nat Rev Mol Cell Bio. 21, 183–203 (2020). [PubMed: 31937935]
33. Zan ED, van Stiphout R, Gapp BV, Blomen VA, Brummelkamp TR, Nijman SMB, Quantitative genetic screening reveals a Ragulator-FLCN feedback loop that regulates the mTORC1 pathway. Sci Signal. 13, eaba5665 (2020).

34. Condon KJ, Orozco JM, Adelmann CH, Spinelli JB, van der Helm PW, Roberts JM, Kunchok T, Sabatini DM, Genome-wide CRISPR screens reveal multitiered mechanisms through which mTORC1 senses mitochondrial dysfunction. Proc National Acad Sci. 118, e2022120118 (2021).
35. Zhang Z, Liu J, Li M, Yang H, Zhang C, Evolutionary Dynamics of the Interferon-Induced Transmembrane Gene Family in Vertebrates. Plos One. 7, e49265 (2012).
36. Li P, Shi M-L, Shen W-L, Zhang Z, Xie D-J, Zhang X-Y, He C, Zhang Y, Zhao Z-H, Coordinated regulation of IFITM1, 2 and 3 genes by an IFN-responsive enhancer through long-range chromatin interactions. Biochimica Et Biophysica Acta Bba - Gene Regul Mech. 1860, 885–893 (2017).
37. Garnett MJ, Edelman EJ, Heidorn SJ, Greenman CD, Dastur A, Lau KW, Greninger P, Thompson IR, Luo X, Soares J, Liu Q, Iorio F, Surdez D, Chen L, Milano RJ, Bignell GR, Tam AT, Davies H, Stevenson JA, Barthorpe S, Lutz SR, Kogera F, Lawrence K, McLaren-Douglas A, Mitropoulos X, Mironenko T, Thi H, Richardson L, Zhou W, Jewitt F, Zhang T, O'Brien P, Boisvert JL, Price S, Hur W, Yang W, Deng X, Butler A, Choi HG, Chang JW, Baselga J, Stamenkovic I, Engelman JA, Sharma SV, Delattre O, Saez-Rodriguez J, Gray NS, Settleman J, Futreal PA, Haber DA, Stratton MR, Ramaswamy S, McDermott U, Benes CH, Systematic identification of genomic markers of drug sensitivity in cancer cells. Nature. 483, 570–575 (2012). [PubMed: 22460902]
38. Rees MG, Seashore-Ludlow B, Cheah JH, Adams DJ, Price EV, Gill S, Javaid S, Coletti ME, Jones VL, Bodycombe NE, Soule CK, Alexander B, Li A, Montgomery P, Kotz JD, Hon CS-Y, Munoz B, Liefeld T, Dančík V, Haber DA, Clish CB, Bittker JA, Palmer M, Wagner BK, Clemons PA, Shamji AF, Schreiber SL, Correlating chemical sensitivity and basal gene expression reveals mechanism of action. Nat Chem Biol. 12, 109–116 (2016). [PubMed: 26656090]
39. Iorio F, Knijnenburg TA, Vis DJ, Bignell GR, Menden MP, Schubert M, Aben N, Gonçalves E, Barthorpe S, Lightfoot H, Cokelaer T, Greninger P, van Dyk E, Chang H, de Silva H, Heyn H, Deng X, Egan RK, Liu Q, Mironenko T, Mitropoulos X, Richardson L, Wang J, Zhang T, Moran S, Sayols S, Soleimani M, Tamborero D, Lopez-Bigas N, Ross-Macdonald P, Esteller M, Gray NS, Haber DA, Stratton MR, Benes CH, Wessels LFA, Saez-Rodriguez J, McDermott U, Garnett MJ, A Landscape of Pharmacogenomic Interactions in Cancer. Cell. 166, 740–754 (2016). [PubMed: 27397505]
40. Adamson B, Norman TM, Jost M, Cho MY, Nuñez JK, Chen Y, Villalta JE, Gilbert LA, Horlbeck MA, Hein MY, Pak RA, Gray AN, Gross CA, Dixit A, Parnas O, Regev A, Weissman JS, A Multiplexed Single-Cell CRISPR Screening Platform Enables Systematic Dissection of the Unfolded Protein Response. Cell. 167, 1867–1882.e21 (2016). [PubMed: 27984733]
41. Stockwell BR, Chemical genetics: ligand-based discovery of gene function. Nat Rev Genet. 1, 116–125 (2000). [PubMed: 11253651]
42. Brass AL, Huang I-C, Benita Y, John SP, Krishnan MN, Feeley EM, Ryan BJ, Weyer JL, van der Weyden L, Fikrig E, Adams DJ, Xavier RJ, Farzan M, Elledge SJ, The IFITM Proteins Mediate Cellular Resistance to Influenza A H1N1 Virus, West Nile Virus, and Dengue Virus. Cell. 139, 1243–1254 (2009). [PubMed: 20064371]
43. Bailey CC, Zhong G, Huang I-C, Farzan M, IFITM-Family Proteins: The Cell's First Line of Antiviral Defense. Annual Review of Virology. 1, 1–23 (2014).
44. Shi G, Schwartz O, Compton AA, More than meets the I: the diverse antiviral and cellular functions of interferon-induced transmembrane proteins. Retrovirology. 14, 53 (2017). [PubMed: 29162141]
45. Zhao X, Li J, Winkler CA, An P, Guo J-T, IFITM Genes, Variants, and Their Roles in the Control and Pathogenesis of Viral Infections. Frontiers in Microbiology. 9, 3228 (2019). [PubMed: 30687247]
46. Li K, Markosyan RM, Zheng Y-M, Golfetto O, Bungart B, Li M, Ding S, He Y, Liang C, Lee JC, Gratton E, Cohen FS, Liu S-L, IFITM Proteins Restrict Viral Membrane Hemifusion. Plos Pathog. 9, e1003124 (2013).
47. Zhao X, Guo F, Liu F, Cuconati A, Chang J, Block TM, Guo J-T, Interferon induction of IFITM proteins promotes infection by human coronavirus OC43. Proc National Acad Sci. 111, 6756–6761 (2014).
48. Lee J, Robinson ME, Ma N, Artadji D, Ahmed MA, Xiao G, Sadras T, Deb G, Winchester J, Cosgun KN, Geng H, Chan LN, Kume K, Miettinen TP, Zhang Y, Nix MA, Klemm L, Chen CW, Chen J, Khairnar V, Wiita AP, Thomas-Tikhonenko A, Farzan M, Jung JU, Weinstock DM,

Manalis SR, Diamond MS, Vaidehi N, Müschen M, IFITM3 functions as a PIP3 scaffold to amplify PI3K signalling in B cells. Nature, 1–7 (2020).

49. Buchrieser J, Degrelle SA, Couderc T, Nevers Q, Disson O, Manet C, Donahue DA, Porrot F, Hillion K-H, Perthame E, Arroyo MV, Souquere S, Ruigrok K, Dupressoir A, Heidmann T, Montagutelli X, Fournier T, Lecuit M, Schwartz O, IFITM proteins inhibit placental syncytiotrophoblast formation and promote fetal demise. Sci New York N Y. 365, 176–180 (2019).
50. Spence JS, He R, Hoffmann H-H, Das T, Thinon E, Rice CM, Peng T, Chandran K, Hang HC, IFITM3 directly engages and shuttles incoming virus particles to lysosomes. Nat Chem Biol. 15, 259–268 (2019). [PubMed: 30643282]
51. . Das T, Yang X, Lee H, Garst EH, Valencia E, Chandran K, Im W, Hang HC, S-Palmitoylation and Sterol Interactions Mediate Antiviral Specificity of IFITMs. Acs Chem Biol. 17, 2109–2120 (2022). [PubMed: 35861660]
52. Epstein FH, Kurzrock R, Gutterman JU, Talpaz M, The Molecular Genetics of Philadelphia Chromosome–Positive Leukemias. New Engl J Medicine. 319, 990–998 (1988).
53. Schindler T, Bornmann W, Pellicena P, Miller WT, Clarkson B, Kuriyan J, Structural Mechanism for STI-571 Inhibition of Abelson Tyrosine Kinase. Science. 289, 1938–1942 (2000). [PubMed: 10988075]
54. Braun TP, Eide CA, Druker BJ, Response and Resistance to BCR-ABL1-Targeted Therapies. Cancer Cell. 37, 530–542 (2020). [PubMed: 32289275]
55. Zhang J, Adrián FJ, Jahnke W, Cowan-Jacob SW, Li AG, Iacob RE, Sim T, Powers J, Dierks C, Sun F, Guo G-R, Ding Q, Okram B, Choi Y, Wojciechowski A, Deng X, Liu G, Fendrich G, Strauss A, Vajpai N, Grzesiek S, Tuntland T, Liu Y, Bursulaya B, Azam M, Manley PW, Engen JR, Daley GQ, Warmuth M, Gray NS, Targeting Bcr–Abl by combining allosteric with ATP-binding-site inhibitors. Nature. 463, 501–506 (2010). [PubMed: 20072125]
56. Wylie AA, Schoepfer J, Jahnke W, Cowan-Jacob SW, Loo A, Furet P, Marzinzik AL, Pelle X, Donovan J, Zhu W, Buonamici S, Hassan AQ, Lombardo F, Iyer V, Palmer M, Berellini G, Dodd S, Thohan S, Bitter H, Branford S, Ross DM, Hughes TP, Petruzzelli L, Vanasse KG, Warmuth M, Hofmann F, Keen NJ, Sellers WR, The allosteric inhibitor ABL001 enables dual targeting of BCR–ABL1. Nature. 543, 733–737 (2017). [PubMed: 28329763]
57. Iacob RE, Zhang J, Gray NS, Engen JR, Allosteric Interactions between the Myristate- and ATP-Site of the Abl Kinase. Plos One. 6, e15929 (2011).
58. Vajpai N, Strauss A, Fendrich G, Cowan-Jacob SW, Manley PW, Grzesiek S, Jahnke W, Solution Conformations and Dynamics of ABL Kinase-Inhibitor Complexes Determined by NMR Substantiate the Different Binding Modes of Imatinib/Nilotinib and Dasatinib* ♦. J Biol Chem. 283, 18292–18302 (2008). [PubMed: 18434310]
59. Fabian MA, Biggs WH, Treiber DK, Atteridge CE, Azimioara MD, Benedetti MG, Carter TA, Ciceri P, Edeen PT, Floyd M, Ford JM, Galvin M, Gerlach JL, Grotzfeld RM, Herrgard S, Insko DE, Insko MA, Lai AG, Lélias J-M, Mehta SA, Milanov ZV, Velasco AM, Wodicka LM, Patel HK, Zarrinkar PP, Lockhart DJ, A small molecule–kinase interaction map for clinical kinase inhibitors. Nat Biotechnol. 23, 329–336 (2005). [PubMed: 15711537]
60. Das J, Chen P, Norris D, Padmanabha R, Lin J, Moquin RV, Shen Z, Cook LS, Doweyko AM, Pitt S, Pang S, Shen DR, Fang Q, de Fex HF, McIntyre KW, Shuster DJ, Gillooly KM, Behnia K, Schieven GL, Wityak J, Barrish JC, 2-Aminothiazole as a Novel Kinase Inhibitor Template. Structure−Activity Relationship Studies toward the Discovery of N -(2-Chloro-6-methylphenyl)-2-[[6-[4-(2-hydroxyethyl)-1- piperazinyl)]-2-methyl-4-pyrimidinyl]amino)]-1,3-thiazole-5-carboxamide (Dasatinib, BMS-354825) as a Potent pan -Src Kinase Inhibitor. J Med Chem. 49, 6819–6832 (2006). [PubMed: 17154512]
61. Gower CM, Chang MEK, Maly DJ, Bivalent inhibitors of protein kinases. Crit Rev Biochem Mol. 49, 102–115 (2014).
62. Zhao Q, Ouyang X, Wan X, Gajiwala KS, Kath JC, Jones LH, Burlingame AL, Taunton J, Broad-Spectrum Kinase Profiling in Live Cells with Lysine-Targeted Sulfonyl Fluoride Probes. Journal of the American Chemical Society. 139, 680–685 (2017). [PubMed: 28051857]
63. Cravatt BF, Wright AT, Kozarich JW, Activity-Based Protein Profiling: From Enzyme Chemistry to Proteomic Chemistry. Annu Rev Biochem. 77, 383–414 (2008). [PubMed: 18366325]

64. Iwasaki S, Floor SN, Ingolia NT, Rocaglates convert DEAD-box protein eIF4A into a sequence-selective translational repressor. Nature. 534, 558 (2016). [PubMed: 27309803]

65. Iwasaki S, Iwasaki W, Takahashi M, Sakamoto A, Watanabe C, Shichino Y, Floor SN, Fujiwara K, Mito M, Dodo K, Sodeoka M, Imataka H, Honma T, Fukuzawa K, Ito T, Ingolia NT, The Translation Inhibitor Rocaglamide Targets a Bimolecular Cavity between eIF4A and Polypurine RNA. Mol Cell. 73, 738–748.e9 (2019). [PubMed: 30595437]

66. Dobson CM, Chemical space and biology. Nature. 432, 824–828 (2004). [PubMed: 15602547]

67. Wassarman DR, dwassarman/cellpanelr: v0.0.0.9001, Zenodo (2022); 10.5281/zenodo.7191410.

68. Horlbeck MA, Xiong X, Jost M, mhorlbeck/ScreenProcessing: v0.1, Zenodo (2022); 10.5281/zenodo.7185885.

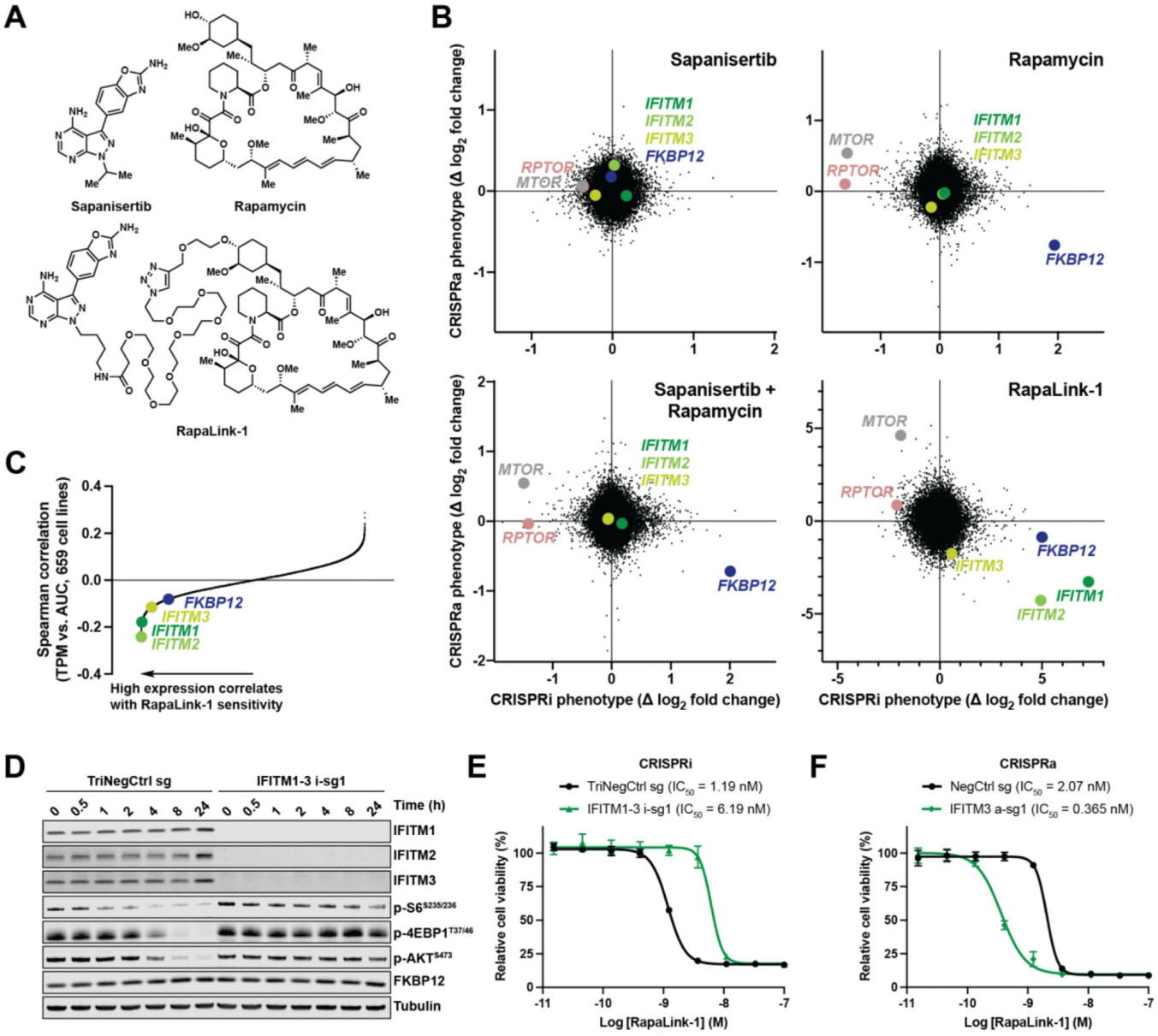

Fig. 1. IFITMs promote the cellular activity of a bitopic MTOR inhibitor.

(**A**) Chemical structures of MTOR inhibitors. (**B**) Gene phenotypes from genome-scale CRISPRi and CRISPRa screens in K562 cells. Genes involved in MTOR complex 1 (*MTOR* and *RPTOR*), a requisite rapamycin inhibitory complex partner (*FKBP12*), and clade I IFITMs (*IFITM1*, *IFITM2*, and *IFITM3*) are highlighted. Data represent two biological replicates. (**C**) Spearman correlation coefficients between RapaLink-1 sensitivity, as measured by dose-response data, and transcript abundance, as measured by RNA sequencing (see also fig. S4). Dose-response data are expressed as area under the curve (AUC) and RNA sequencing data are expressed as transcripts per million (TPM). Genes are highlighted as in (B). (**D**) Immunoblots of K562 CRISPRi cells expressing sgRNAs treated with RapaLink-1 (3 nM) for the times indicated. (**E** and **F**) Viability of K562 CRISPRi (E)

or CRISPRa (F) cells expressing sgRNAs treated with RapaLink-1. Data represent means of three biological replicates; error bars denote SD.

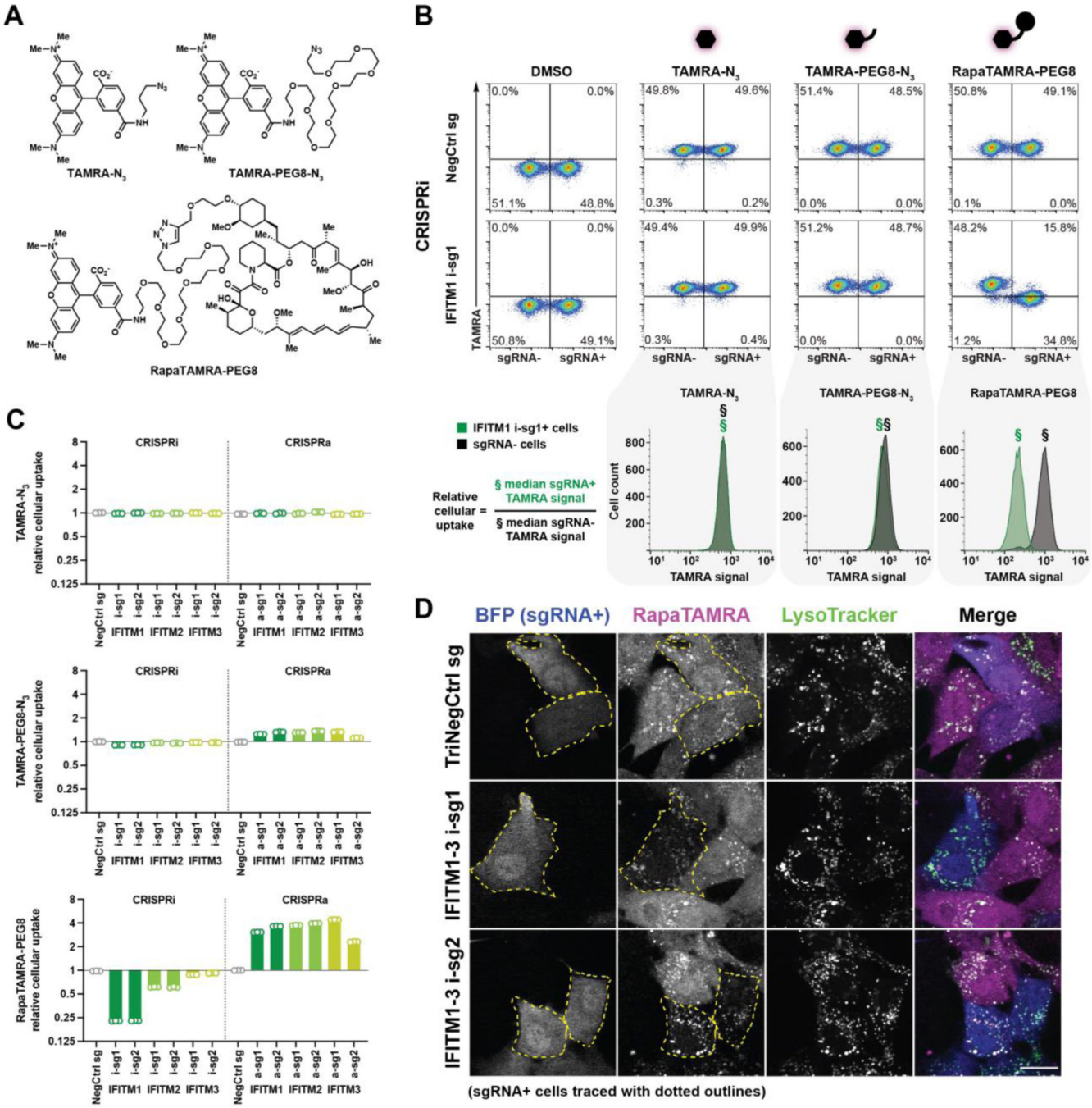

Fig. 2. IFITMs promote the cellular uptake of linked chemotypes.

(**A**) Chemical structures of fluorescent RapaLink-1 analogs. (**B**) Measurement of fluorescent molecule uptake in K562 CRISPRi cells expressing sgRNAs (sgRNA+). Cells were incubated with TAMRA-N_3 (10 nM), TAMRA-PEG8-N_3 (1 μM), or RapaTAMRA-PEG8 (1 nM) for 24 h. Uptake modulation by sgRNAs was quantified by internal normalization to non-transduced cells (sgRNA-) present within the mixture (i.e. relative cellular uptake). Data representative of three biological replicates. (**C**) Changes in uptake of fluorescent molecules by sgRNAs targeting *IFITM1–3* as in (B and fig. S6A). Relative cellular uptake < 1

indicates decreased uptake and > 1 indicates increased uptake. Data represent means of three biological replicates. (**D**) Confocal microscopy images of RPE-1 CRISPRi cells expressing indicated sgRNAs (blue) and treated for 24 h with RapaTAMRA-PEG8 (magenta) and LysoTracker (green). sgRNA+ cells are traced with dotted outlines (yellow) in left two columns for clarity. Scale bar denotes 20 μm.

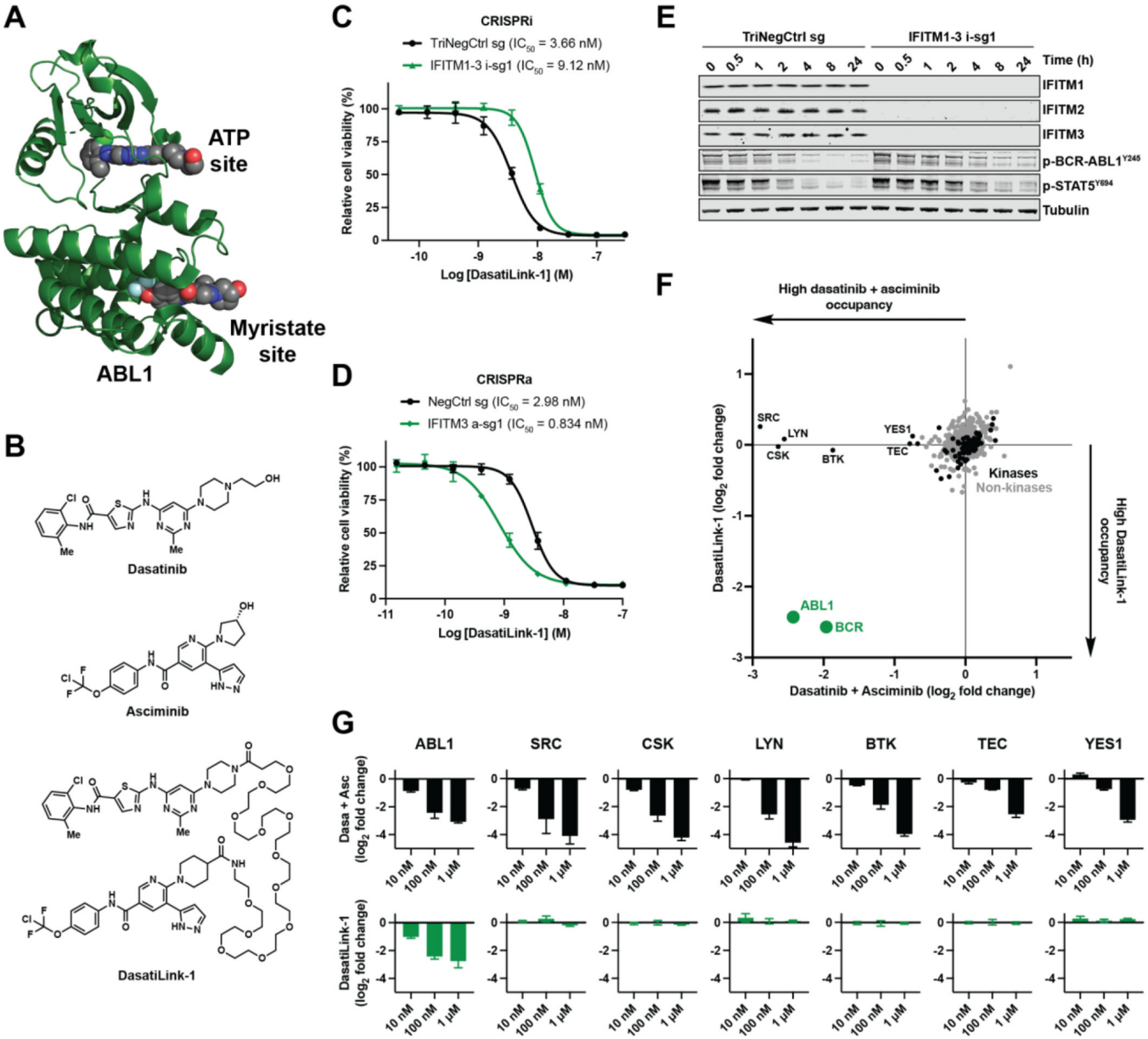

Fig. 3. Design and characterization of an IFITM-assisted bitopic BCR-ABL1 inhibitor.

(**A**) Molecular model of ABL1 kinase domain. The model was constructed by aligning two crystal structures: one bound to dasatinib (PDB, 2GQG) and one bound to asciminib (PDB, 5MO4). (**B**) Chemical structures of BCR-ABL1 inhibitors. (**C** and **D**) Viability of K562 CRISPRi (C) or CRISPRa (D) cells expressing sgRNAs treated with DasatiLink-1. Data represent means of three biological replicates; error bars denote SD. (**E**) Immunoblots of K562 CRISPRi cells expressing sgRNAs treated with DasatiLink-1 (5 nM) for the times indicated (**F**) In-cell kinase occupancy profiling of DasatiLink-1 and an unlinked control (a 1:1 mixture of dasatinib and asciminib) at equimolar concentration (100 nM). Data represent means of three biological replicates. (**G**) As in (F) for kinases occupied following 10 nM, 100 nM, and 1 μM inhibitor treatments; error bars denote SD.

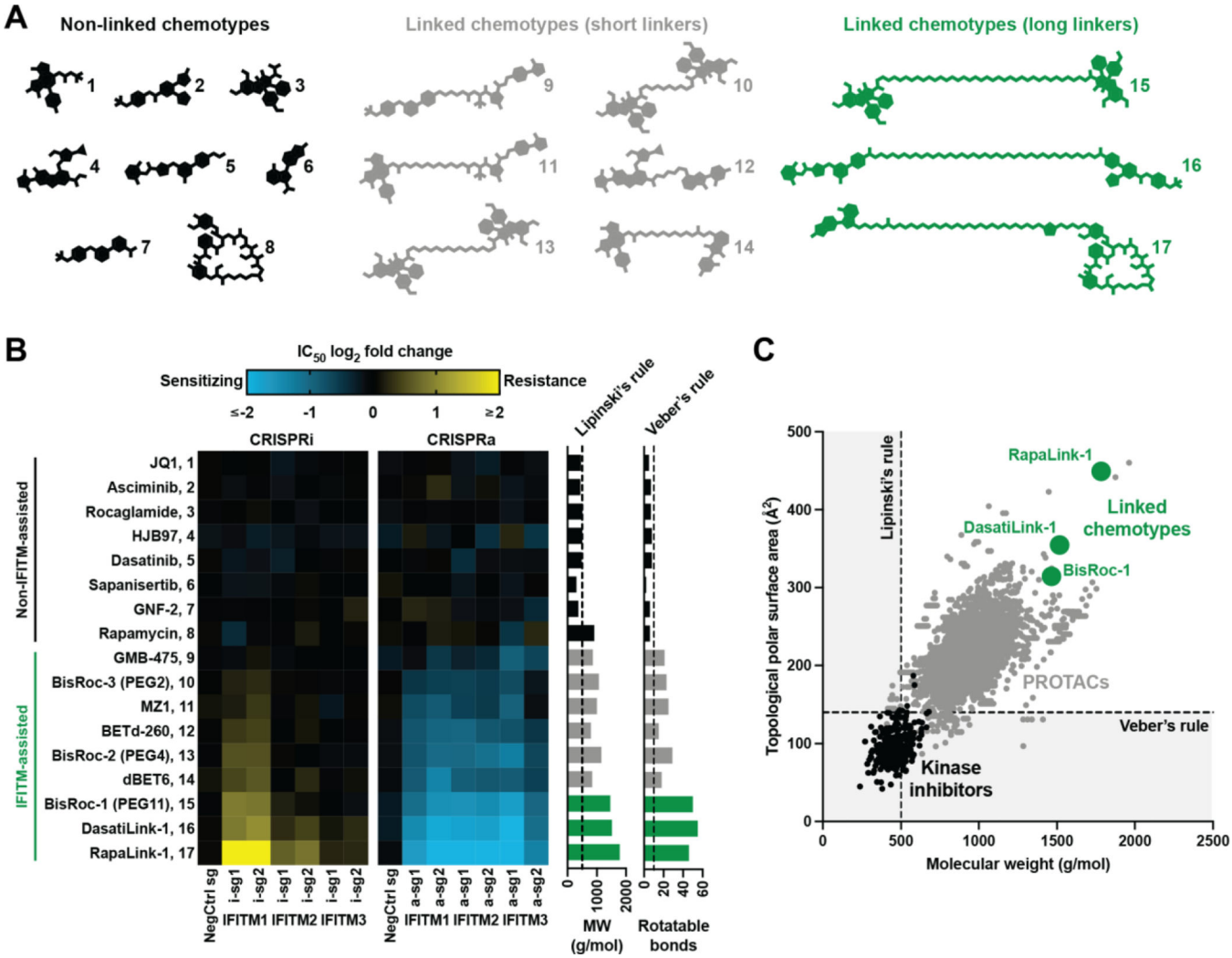

Fig. 4. IFITMs assist the cellular activity of diverse linked chemotypes.

(**A**) Heavy atom skeletons of compounds assessed for IFITM assistance (see also fig. S10 for chemical structures). Compounds were categorized as non-linked chemotypes (compounds 1–8, black), linked chemotypes with short linkers (compounds 9–14, gray), or linked chemotypes with long linkers (compounds 15–17, green). (**B**) Chemical-genetic interaction map of inhibitors in (A) with *IFITM1*, *IFTM2*, and *IFITM3*. Potency, as measured by dose-response IC_{50} in a cell viability assay (see also Fig. 1F, Fig. 3D, or fig. S9D for example source data), was normalized to that of non-sgRNA-expressing K562 CRISPRi or CRISPRa cells. Physicochemical properties, including molecular weight (MW) and number of rotatable bonds, with their respective traditional thresholds for drug-likeness are indicated (right). Data represent means of three biological replicates. (**C**) Map of chemical space populated by 304 kinase inhibitors in clinical development (black), 3270 PROTACs reported in the literature (gray), and 3 linked chemotypes described herein (green). Boundaries represent traditional guidelines for drug-likeness.